IJNAOE
©SNAK, 2015

Int. J. Nav. Archit. Ocean Eng. (2015) 7:580~594
http://dx.doi.org/10.1515/ijnaoe-2015-0041
pISSN: 2092-6782, eISSN: 2092-6790

Effect of natural frequency modes on sloshing phenomenon in a rectangular tank

Jae Hwan Jung[1], Hyun Sik Yoon[2] and Chang Yeol Lee[3]

[1]*Department of Naval Architecture and Ocean Engineering, Pusan National University, Busan, Korea*
[2]*Global Core Research Center for Ships and Offshore Plants, Pusan National University, Busan, Korea*
[3]*Department of Hyundai Maritime Research Institute, Hyundai Heavy Industries, Ulsan, Korea*

Received 25 July 2014; Revised 19 November 2014; Accepted 26 March 2015

ABSTRACT: *Liquid sloshing in two-dimensional (2-D) and three-dimensional (3-D) rectangular tanks is simulated by using a level set method based on the finite volume method. In order to examine the effect of natural frequency modes on liquid sloshing, we considered a wide range of frequency ratios (*$0.5 \le fr \le 3.2$*). The frequency ratio is defined by the ratio of the excitation frequency to the natural frequency of the fluid, and covers natural frequency modes from 1 to 5. When* $fr = 1$*, which corresponds to the first mode of the natural frequency, strong liquid sloshing reveals roof impact, and significant forces are generated by the liquid in the tank. The liquid flows are mainly unidirectional. Thus, the strong bulk motion of the fluid contributes to a higher elevation of the free surface. However, at* $fr = 2$*, the sloshing is considerably suppressed, resulting in a calm wave with relatively lower elevation of the free surface, since the waves undergo destructive interference. At* $fr = 2$*, the lower peak of the free surface elevation occurs. At higher modes of* fr_3*,* fr_4*, and* fr_5*, the free surface reveals irregular deformation with nonlinear waves in every case. However, the deformation of the free surface becomes weaker at higher natural frequency modes. Finally, 3-D simulations confirm our 2-D results.*

KEY WORDS: Liquid sloshing; Natural frequency modes; Level set method.

INTRODUCTION

In the past several years, because of increased demand for natural gas and related products, the demand for Liquefied Natural Gas (LNG) container ships has been rapidly rising. In response to this fact, stringent regulations are forcing the shipping industry to develop a ship design that can meet safety standards and prevent explosion accidents of LNG cargo tanks. Liquid sloshing, which can cause severe structural damage that results in a subsequent explosion of the cargo tank, has attracted considerable attention. In addition, liquid sloshing in a transport system is associated with various engineering problems such as transporting vehicle on highways, sloshing of liquid cargo in LNG container ship, and the motion of liquid fuel in aircraft and spacecraft (Wu and Chen, 2009). Therefore, an understanding of the sloshing mechanism is very important in engineering applications.

Corresponding author: *Hyun Sik Yoon*, e-mail: *lesmodel@pusan.ac.kr*

It is known that liquid in partially-filled tanks tends to experience sloshing under certain conditions. When the frequency of the tank motion is close to the natural frequency of the liquid in the tank, localized high impact loads on the tank walls occur due to extreme liquid motion (Bass et al., 1980). Therefore, sloshing phenomena must be investigated in tank designs (Akyildiz and Unal, 2005; Kim, 2013; Kim et al., 2005; Lee et al., 2013; Lee, 2014). Many researchers have investigated sloshing phenomena using various analytic, numerical, and experimental approaches, and these studies have revealed many significant phenomena in recent decades.

The potential formulation is often used in sloshing studies. This approach provides a simplified means of evaluating sloshing, but its use is limited in the case of real nonlinear fluid problems. For example, for cases involving shallow-filled tanks with internal baffles, potential flow theory is not sufficiently reliable (Armenio and Rocca, 1996; Faltinsen, 1987; Wiesche, 2003). In addition to the potential flow approaches, many numerical studies based on Navier-Stokes (NS) equations have been performed to overcome the aforementioned problem. Also, the calculation of the free surface profile inside a tank is a key factor in the accurate approximation of loads generated by sloshing. As a result, many studies have been conducted using Two-Dimensional (2-D) and Three-Dimensional (3-D) simulations with the use of free-surface capturing models such as the Marker and Cell (MAC) approach, the Volume of Fluid method (VOF), and the Level Set Method (LSM), or a combination of LSM and VOF (Rhee, 2005; Price and Chen, 2006; Jung et al., 2012). Also, recently, the Smoothed Particle Hydrodynamics (SPH) approach has been quite successful (Delorme et al., 2009; Bouscasse et al., 2013) in simulating 2-D sloshing flows.

Using numerical tools, investigators have examined characteristics of sloshing phenomena that depend on design variables such as liquid depth, tank geometry, the frequency and amplitude of external excitation, and the position of the Center of Gravity (CG). To suppress extreme sloshing, it is important to carefully consider these design variables. One of the solutions used to prevent extreme free surface fluctuations is to install baffles inside a liquid tank (Ibrahim, 2005). Many researchers have successfully demonstrated that installing baffles is useful in reducing the pressure loads on the walls or ceiling of a tank in combination with suppressing extreme fluid motion, using numerical simulation based on the NS equations. The filling level in the tanks is also a key element. The largest sloshing loads tend to occur at filling level (h) and tank length (L) filling ratios of $0.1 \le h/L \le 0.5$ (MacDonald and Maguire, 2008).

Most of the aforementioned studies focused on a frequency of external excitation that is close to the natural frequency. However, to our knowledge, it is hard to find reports that describe a wide frequency ratio range for sloshing in 2-D and 3-D tanks, and especially for viscous flow conditions. Recently, Bouscasse et al. (2013) focused on sway motion (horizontal amplitude excitation) and considered a broad range of frequencies, filling conditions, and amplitude excitations. However, the filling ratios they examined are quite small (to satisfy the shallow water regimes). A narrow tank has been used to limit 3-D effects and allow for an extensive study of 2-D waves

In the present study, we considered a wide range of frequency of tank motion in order to investigate the effect of the excitation frequency on sloshing phenomena in a rectangular tank. Special attention was devoted to free surface deformation and elevation for the case in which the excitation frequency of the tank is the same as a natural frequency and corresponding mode of the fluid. Therefore, for the natural frequency modes, we performed additional numerical simulations for sloshing in a 3-D tank to clarify the 2-D results of our simulation.

NUMERICAL DETAILS

Governing equations

For unsteady incompressible viscous flow of two immiscible fluids, the governing equations are the continuity and momentum equations. In a rectangular coordinate system, these equations can be expressed as

$$\frac{\partial u_i}{\partial x_i} = 0 \tag{1}$$

$$\frac{\partial u_i}{\partial t} + u_j \frac{\partial u_i}{\partial x_j} = -\frac{1}{\rho}\frac{\partial p}{\partial x_i} + \nu \frac{\partial^2 u_i}{\partial x_j \partial x_j} + g_i + f_i \tag{2}$$

where t is the time, u_i is the velocity vector, ρ is the fluid density, p is the pressure, v is the kinematic viscosity of the fluid, f is the external force, and g is the gravitational acceleration.

Level set method

We used the LSM to capture the large deformation and extreme behavior of the interface of two-phase flows. Defining the interface as the zero level set of a signed distance function ϕ, or the level set function, the position of the interface can be tracked by solving the level set evolution equation (Osher and Sethian, 1988):

$$\frac{\partial \phi}{\partial t} + u \cdot \nabla \phi = 0 \tag{3}$$

The level set equation is solved over the entire computational domain, including the fluid and solid zones. The reinitialization equation (Sussman et al., 1994) for the level set function is iteratively solved to keep ϕ as a signed distance function in the course of its evolution:

$$\frac{\partial \phi}{\partial \tau} + S(\phi_0)(|\nabla \phi| - 1) = 0 \tag{4}$$

where τ is the pseudo-time for the iteration and $S(\phi_0)$ is the numerically smeared-out sign function, given by

$$S(\phi_0) = \frac{\phi_0}{\sqrt{\phi_0^2 + (\Delta h)^2}} \tag{5}$$

where ϕ_0 is the initial value of ϕ, and Δh is a small amount, usually the grid cell size, to smear out the sign function.

Because the level set function is a signed distance function, the unit normal vector, n, and the local curvature, κ, of the interface can be readily calculated by applying the standard finite difference approach to the level set function as follows:

$$n = \frac{\nabla \phi}{|\nabla \phi|} \tag{6}$$

and

$$\kappa = \nabla \cdot n = \nabla \cdot \frac{\nabla \phi}{|\nabla \phi|} \tag{7}$$

Each phase of constant density and viscosity can be easily defined by the level set function in the computational domain, and sharp jumps of the fluid properties occur at the phase interface. We chose to regularize the viscosity and density with a smoothed Heaviside function across the interface. The density and viscosity were smoothed over a transition band across the interface as follows:

$$\rho(\phi) = \rho_G + (\rho_L - \rho_G) H(\phi) \tag{8}$$

$$\mu(\phi) = \mu_G + (\mu_L - \mu_G)H(\phi) \tag{9}$$

where the subscripts G and L represent the gas phase and liquid phase, respectively. The smoothed Heaviside function (Sussman et al., 1994) is defined as

$$H(\phi) = \begin{cases} 1, & if\ \phi > \varepsilon \\ \frac{1}{2}\left[1 + \frac{\phi}{\varepsilon} + \frac{1}{\pi}\sin\left(\frac{\pi\phi}{\varepsilon}\right)\right], & if\ |\phi| \le \varepsilon \\ 0, & if\ \phi < \varepsilon \end{cases} \tag{10}$$

Numerical methods

The discretization equations can be obtained by integrating the governing equation over the control volume in which the computational nodes are placed at the centers of the control volume. A second-order accuracy finite volume method was used for the spatial discretization in this study. The fractional step method was used for the time advancement of the flow field. This scheme is based on the work of Choi and Moin (1994). The diffusion terms are treated implicitly using the Crank-Nicolson scheme.

To prevent oscillations of the solutions that can arise from steepness gradients of the conservative quantities when the grid is too coarse, in general, first-order or higher-order difference methods belonging to the upwind scheme series were used to approximate the convection terms. A third-order Quadratic Upwind Interpolation for Convective Kinematics (QUICK) scheme (Leonard, 1979) was used for the convective terms. A fifth-order Weighted Essentially Non-Oscillatory (WENO) scheme (Jiang and Peng, 2000) was used for the spatial discretization of the level set evolution and re-initialization equations.

Computational domain and tank motion

Fig. 1 shows a schematic diagram of 2-D and 3-D rectangular tanks containing a liquid, and the locations of probes used to monitor the pressure variation with time. The dimensions of the tank are 0.8 *m* in length (*L*), 0.5 *m* in height (*H*), and 0.4 *m* in breadth (*B*). For all the cases considered in this study, the water depth or filling level (*h*) is 30% of the tank height.

The tank motion is pure surge (translation in the x-direction only), which follows a sinusoidal function given by

$$x_T = A \cdot \sin(\omega_T t) \tag{11}$$

where A and ω_T are the amplitude and the frequency, respectively. In the present study, we considered the amplitude of excitation (A/L) of 0.025. For a given rectangular tank, the natural frequencies of the fluid are given by

$$\omega_n = \sqrt{\frac{n\pi g}{L}\tanh(\frac{n\pi h}{L})} \tag{12}$$

where L is the tank length, h is the water depth, and n is the mode number. Because of the nonlinear feature of the sloshing problem, resonance does not occur exactly at the natural frequency of the fluid as computed using Eq. (12) with mode number n=1, but at a frequency very close to that value (Akyildiz and Unal, 2006). To investigate the effect of the excitation frequency on the sloshing phenomena in a rectangular tank, we considered various frequency mode numbers of the fluid in the tank, as listed in Table 1.

Table 1 Natual frequencies for modes 1-5.

n	ω_n	fr
1	4.513	1 (fr_1)
2	7.977	1.76 (fr_2)
3	10.435	2.31 (fr_3)
4	12.296	2.72 (fr_4)
5	13.833	3.06 (fr_5)

Grid dependency test and validation

In order to test the grid dependence of the solutions and to verify the present numerical methods, we duplicated the same problem conditions as in the experiment of Kang and Lee (2005). They considered a rectangular tank with the same dimensions as in the configuration shown in Fig. 1, with the tank motion governed by Eq. (11) with $\omega_T = \omega_1$. Chen et al. (2009) investigated liquid sloshing numerically under the same problem conditions considered by Kang and Lee (2005) by solving 2-D Reynolds-averaged Navier-Stokes (RANS) equations and adopting the level set method to track the free surface. Three different grid systems (coarse, medium, and fine grids) were considered to test the grid dependence of the solutions, and to validate the present numerical methods as listed in Table 2. Fig. 2 shows the time variations of the pressure for different grid systems, revealing a weak dependence of the solutions on the grid system considered in this study. The results of our computations are in fairly good agreement with previously reported experimental data (Kang and Lee (2005), and with the 2-D simulation results obtained by Chen et al. (2009), regardless of the 2-D and 3-D results, as shown in Fig. 3. Consequently, the medium grid system was selected for all cases.

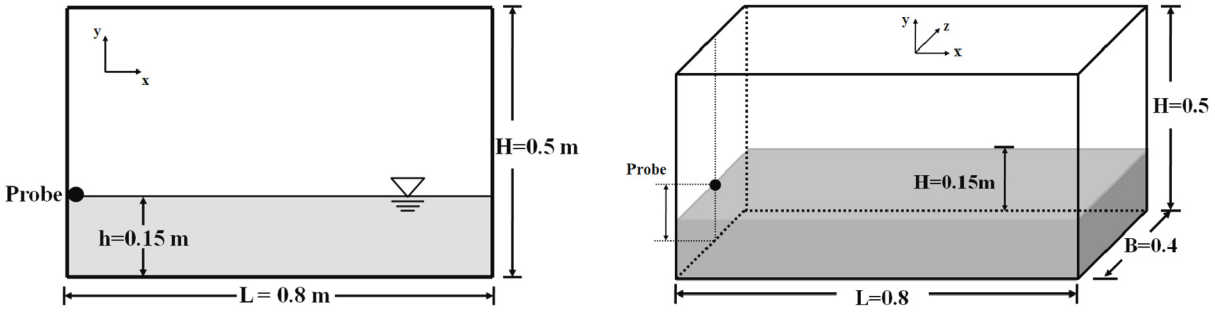

(a) (b)

Fig. 1 Schematics of (a) 2-D and (b) 3-D rectangular tank containing a liquid.

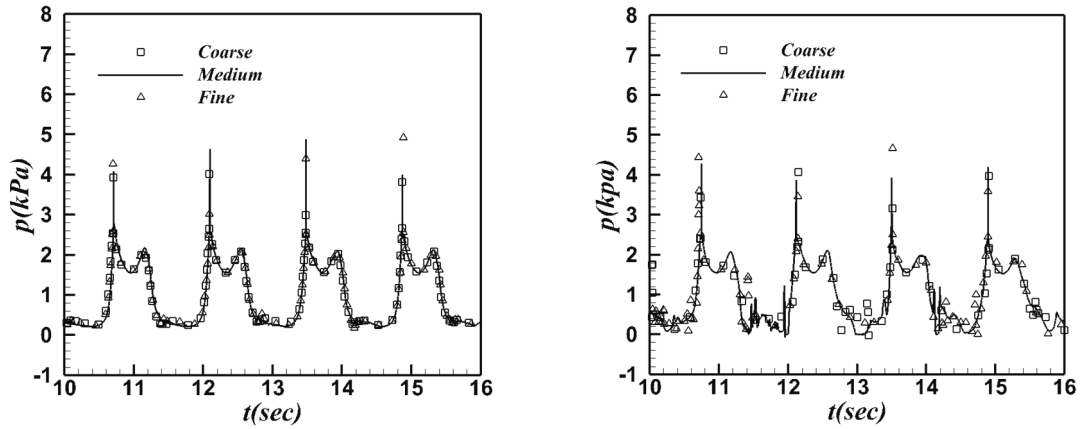

(a) (b)

Fig. 2 Time histories of the pressure for three different grid systems: (a) 2-D and (b) 3-D.

Table 2 Grid dependence test for 2-D and 3-D cases.

Grid system	2-D	3-D
Coarse	100×80	100×80×60
Medium	160×100	160×100×60
Fine	250×120	250×120×60

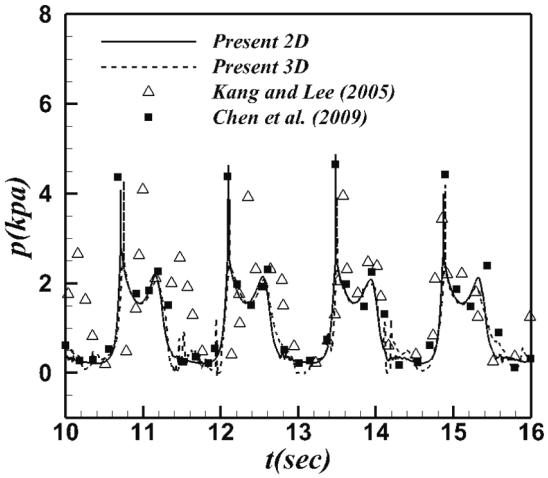

Fig. 3 Comparison of time histories of the pressure with the experimental results of Kang and Lee (2005), and with the numerical results of Chen et al. (2009) at P_T1.

RESULTS AND DISCUSSION

Two-dimensional tank

Free surface deformation

Fig. 4 shows the time evolution of the liquid motion, including the free surface deformation at regular intervals during one period (T) of the tank surge motion for different frequency ratios. Here, representatively, five different frequency ratios of $fr = 1$, 1.76, 2.31, 2.72, and 3.06 were considered, corresponding to fr_1, fr_2, fr_3, fr_4, and fr_5, respectively. In the case of fr_1, strong liquid sloshing is enough to cause the liquid to reach the top wall of the tank after impacting the side walls, leading to extreme sloshing of the liquid in the tank. The liquid flows mainly in the uni-direction. Namely, the fluids of the liquid mainly flow along the same direction, which can be supported by the streamlines. The strong bulk motion of the fluids contributes to a higher elevation of the free surface.

When the frequency ratio increases continuously from fr_1 to fr_2, the sloshing is considerably suppressed, resulting in a calm wave with a relatively lower elevation of the free surface. The liquid flows partially in the same direction as the tank motion, and partially in a direction opposite to the tank motion, which can be seen in the streamlines plotted in Fig. 4(b). Consequently, the waves undergo destructive interference and are suppressed.

As fr increases to fr_3, the free surface reveals the strong irregular deformation accompanying nonlinear waves, which occurs at every instance as shown in Fig. 4(c). This pattern is maintained at the higher modes fr_4 and fr_5, as shown in Figs. 4(d) and (e), respectively. At the high frequency ratios, the fluids cannot quickly turn in the flow direction along the oscillation of the tank because of the inertia of the fluids. Therefore, the liquid flow does not synchronize with the direction of tank motion and does not preserve the uni-direction. Consequently, severe mutual interference of the directions of the fluid flow and tank motion forms irregular waves.

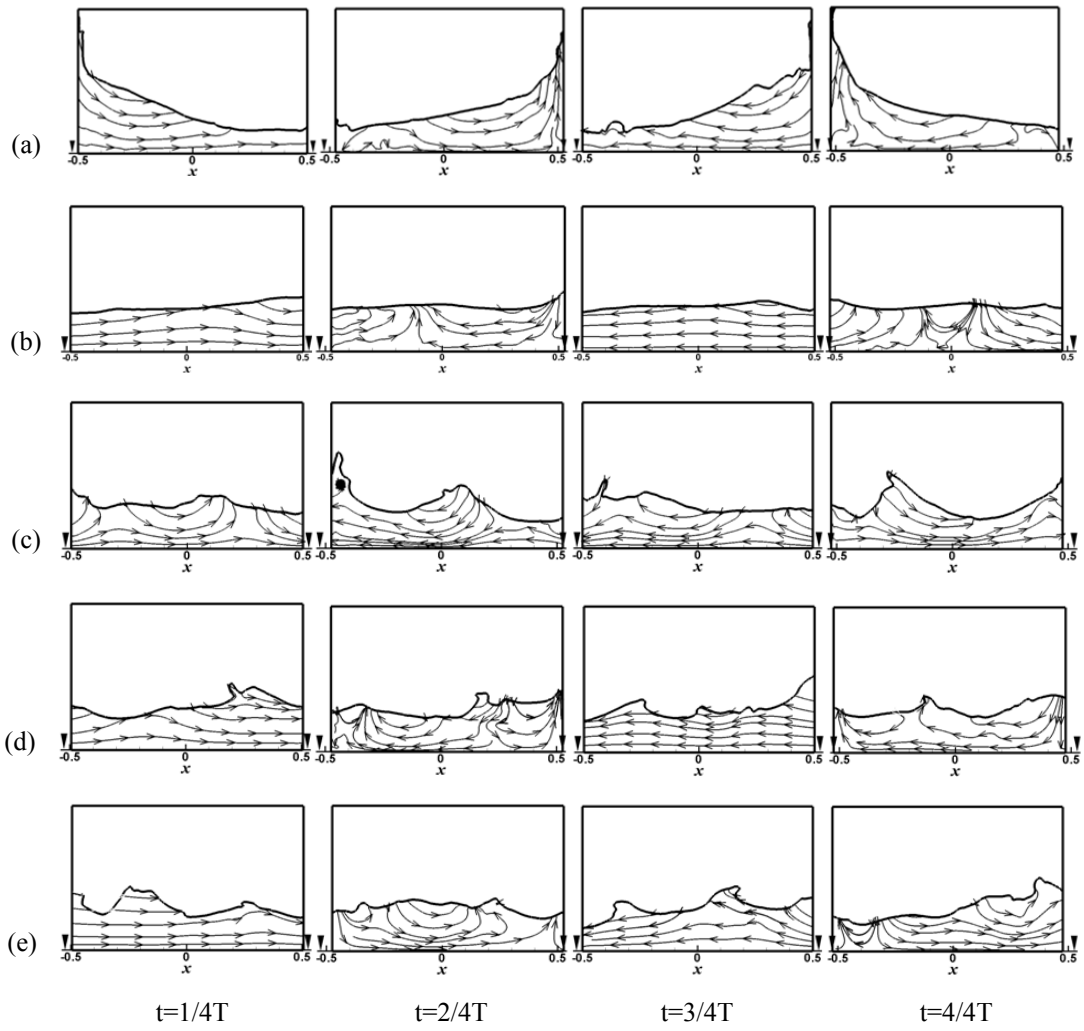

Fig. 4 Phase sequence of streamlines at t=1/4T, t=2/4T, t=3/4T, and t=4/4T with various natural frequency modes: (a) fr_1, (b) fr_2, (c) fr_3, (d) fr_4, and (e) fr_5.

Free surface elevation

Fig. 5 shows the time histories of the free surface elevation for different frequency ratios. As expected, when increasing the frequency ratio to $fr = 1 = fr_1$, which corresponds to the first mode of the natural frequency of the fluid in the rectangular tank, the oscillation of the free surface elevation is dramatically amplified due to resonance as shown in Fig. 5(a). This is because the energy that the flow absorbs is maximized when the oscillations of the tank are "in phase" with the flow oscillations. The flow tends to absorb more energy when the frequency of its oscillations matches the system's natural frequency of vibration than it does at other frequencies. However, when $fr = fr_2$, which corresponds to the second mode of the natural frequency, the variation of the free surface elevation is not large compared to the free surface elevations of the neighboring frequency ratios, as shown in Fig. 5(b). Namely, at the excitation frequency corresponding to the second mode of the natural frequency, a sudden increase in the amplitude of the free surface elevation does not occur. This is supported by very weak liquid sloshing at the frequency ratio fr_2, as shown in Fig. 4(b). In this case, some of the oscillation energy of the fluid is actually extracted by the opposing force due to the oscillation of the tank. As the frequency increases further from fr_2, the frequency of excitation over a range close to the natural frequencies also affects the rate of sloshing. Thus, when fr_3, fr_4, and fr_5, the free surface elevations are augmented compared with neighboring frequency ratios, as shown in Figs. 5(c) to 5(e), respectively. Based on the aforementioned results for the free surface elevations for different frequency ratios, we suggest that the first mode of the natural frequency of the fluid in the rectangular tank is distinctly the resonant frequency.

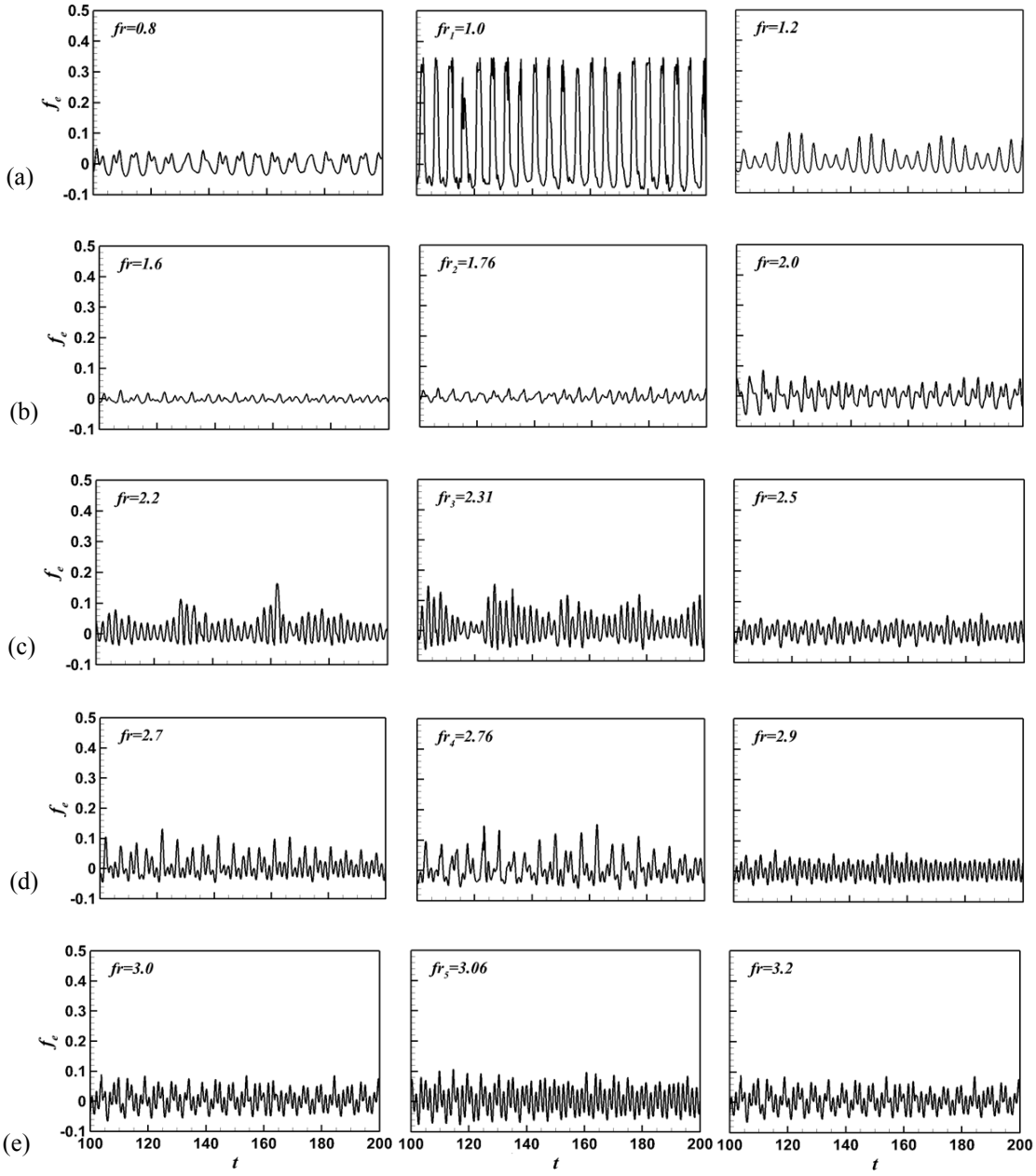

Fig. 5 Time histories of free surface elevation at the probe with various frequency ratios

(a) [$fr = 0.8$, $fr = fr_1$, $fr = 1.2$] (b) [$fr = 1.6$, $fr = fr_2$, $fr = 2.0$] (c) [$fr = 2.2$, $fr = fr_3$, $fr = 2.5$]

(d) [$fr = 2.7$, $fr = fr_4$, $fr = 2.9$] (e) [$fr = 3.0$, $fr = fr_5$, $fr = 3.2$].

Fig. 6 shows the maximum free surface elevation (E_{Max}) as a function of the frequency ratio. The horizontal line in the plots indicates the roof; therefore, the maximum wave height cannot exceed this level. If the maximum wave height reaches this value, then roof impact occurs. When the frequency ratio is in the range of $0.5 \le fr < 0.8$, the free surface elevation is slight. However, as fr increases from 0.8 to 1 (fr_1), the free surface elevates significantly. Eventually, at fr_1 , which is distinctly the resonant frequency, the liquid reaches the roof, which is supported by (as already observed) the free surface deformation shown in Fig. 4(a), and the time history of the free surface elevation shown in Fig. 5(a).

As fr increases from fr_1 to 1.5, the free surface elevation rapidly decreases. When fr increases continuously, the free surface elevation decreases slightly and eventually reaches the local minimum at fr_2 . As fr keeps increasing from fr_2 , the free surface elevation starts to increase again (i.e., recovers), and reaches the second maximum peak at fr_3 .

When fr increases continuously from fr_3 , the free surface elevation decreases and increases alternatively, and the local

peaks at fr_4 and fr_5 correspond to the natural frequency modes. Consequently, under the present conditions of the filling ratio (initial free surface elevation) and the range of the frequency ratio, only fr_1 exhibits roof impact. Therefore, the critical frequency ratio with respect to the roof impact of the free surface is fr_1 except when the liquid does not reach the roof at any instant.

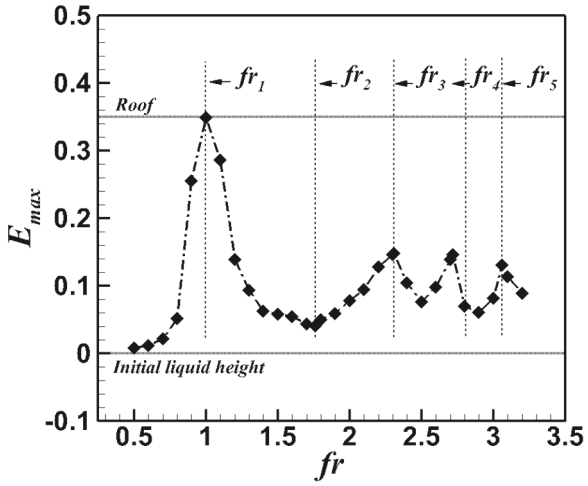

Fig. 6 Maximum free surface elevation ($E_{\max}$) as a function of frequency ratio (fr).

Bouscasse et al. (2013) considered different amplitudes, filling ratios, and frequency ratios, and these filling ratios are smaller than those of the present study. They changed the frequency in order to find the bifurcation. In low filling ratios and small amplitudes, the sloshing is somewhat regular and the bifurcation is easily characterized by an abrupt jump of the free surface. However, in cases of relatively large filling ratios and amplitudes, the bifurcation disappears. The local stochastic behaviors and the low repeatability appear, and the violent impacts are characterized in these cases. In the cases of relatively large filling ratios and amplitudes, the maximum wave elevation appears near the first primary natural frequency when increasing the amplitude, which is consistent with the present results. The wave elevation essentially behaves as a continuous function of the frequency ratio.

Time history and peak wall pressure

The time histories of the wall pressure caused by liquid sloshing at the probe, marked in Fig. 1 for different frequency ratios, are plotted in Fig. 7. As expected from the previous results of the free surface deformation and the elevation of the free surface, when fr becomes $fr_1=1$, the wall pressure at the probe produces very large values compared with those at other values of fr s.

At this value of fr_1, two distinct peaks appear regularly along the time axis, as shown in Fig. 7(a). The first peak occurs at the largest acceleration of the tank, which has the maximum displacement. Subsequently, the first peak is induced by the initial impact of water on the side wall. The second peak, which has about the same magnitude as the first peak, emerges when the falling water hits the underlying liquid. The time of occurrence of the secondary peak is almost the same as when the tank has the opposite maximum displacement, as shown in Fig. 7(a). This pattern of time variation of the pressure is consistent with the results of Peregrine (2003) who shows this double peak behavior as the church roof profile.

When fr becomes 1.2 after $fr_1=1$ of the distinct resonant frequency, the wall pressure at the probe decreases considerably. Even as fr reaches $fr_2=1.76$ as the second mode, the wall pressure at the probe does not recover, and thus exhibits smaller peak values than neighboring frequency ratios, as shown in Fig. 7(b). This is deduced by considering very weak liquid sloshing accompanying a calm free surface, as shown in Figs. 4(b) and 5(b). However, when fr become to be the other modes of the natural frequency of fr_3 , fr_4 , and fr_5 , the peaks of the wall pressure at the probe become larger compared with the neighboring frequency ratios, as shown in Figs. 7(c) to 7(e), respectively.

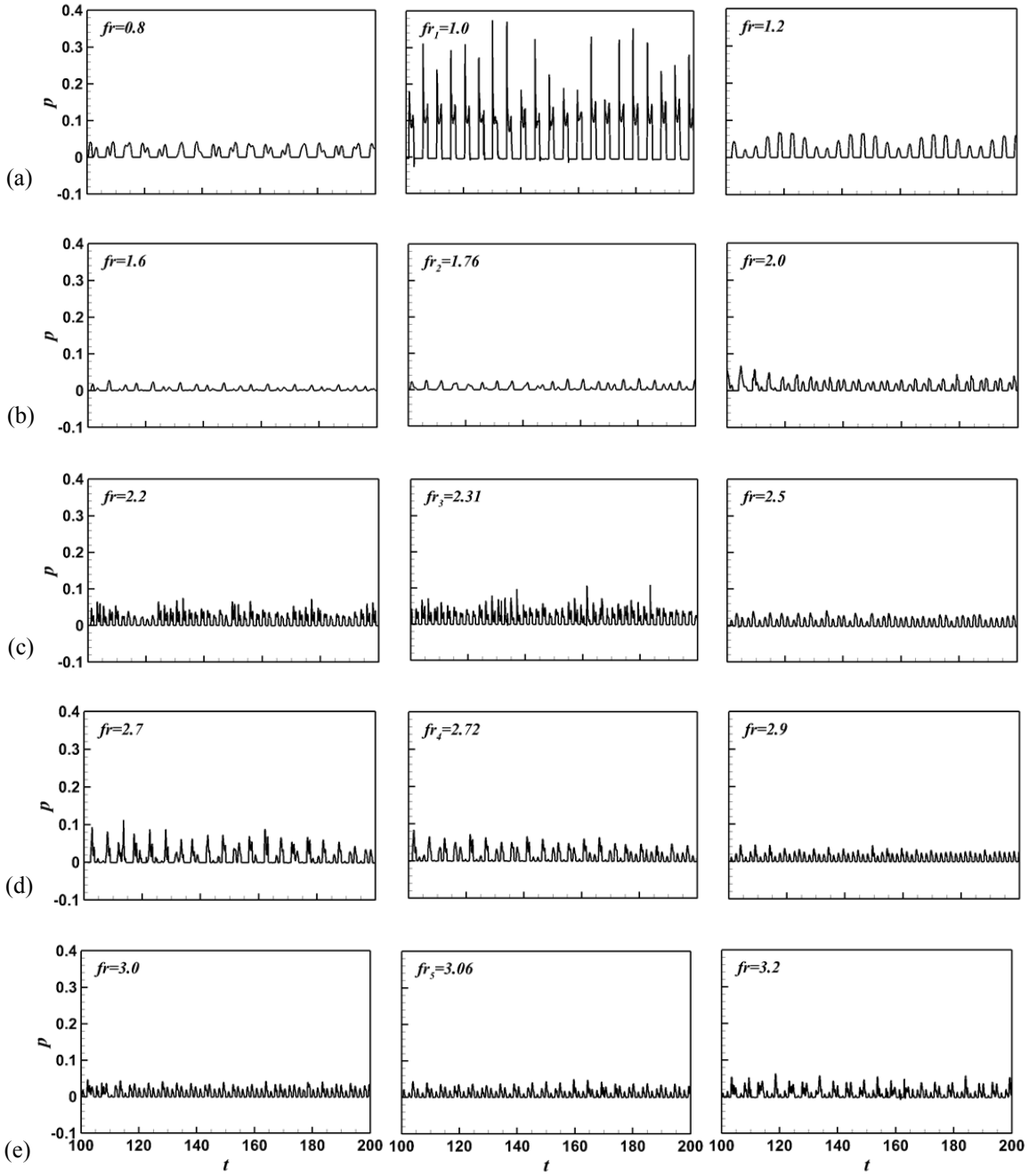

Fig. 7 Time histories of pressure at the probe with various frequency ratios:
(a) [$fr = 0.8$, $fr = fr_1$, $fr = 1.2$] (b) [$fr = 1.6$, $fr = fr_2$, $fr = 2.0$] (c) [$fr = 2.2$, $fr = fr_3$, $fr = 2.5$]
(d) [$fr = 2.7$, $fr = fr_4$, $fr = 2.9$] (e) [$fr = 3.0$, $fr = fr_5$, $fr = 3.2$].

It is essential to know the maximum pressure exerted on the tank wall for the design of the liquid cargo. Thus, the instantaneous peak values in the time histories of the pressure at each probe shown in Fig. 7 were averaged to obtain the mean maximum pressure ($P_{M,Max}$) in relation to the frequency ratio. The mean maximum pressure ($P_{M,Max}$) is achieved by discretely averaging the instantaneous peak values in the time histories of the pressure. The mean maximum pressure variation as a function of frequency ratio is shown in Fig. 8.

The maximum $P_{M,Max}$ occurs at fr_1, which is distinctly the resonant frequency. As fr increases from fr_1 to fr_2, the wall pressure at the probe sharply decreases and reaches the local minimum at fr_2, since the free surface is the most stable at this frequency, as discussed early in the phase sequence of the streamlines and the free surface shown in Fig. 4.

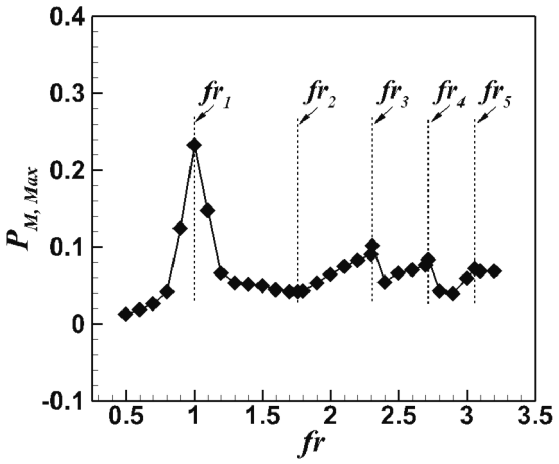

Fig. 8 Variation of averaged maximum pressure according to frequency ratios.

As fr keeps increasing from fr_2, the wall pressure at the probe starts to recover and reaches the second maximum peak at fr_3. When fr increases continuously from fr_3, the wall pressure at the probe decreases and increases alternatively, with the local peaks at fr_4 and fr_5 corresponding to the natural frequency modes, as shown in Fig. 8. This dependence of wall pressure at the probe on the frequency ratio coincides with that of the free surface elevation, as shown in Fig. 6.

In conclusion, the time histories of the wall pressure and the maximum pressure exerted on the tank wall depends strongly on the wave configurations and free surface formations, which depend on the frequency ratios. The relation between the wall pressure and the wave mode can be founded in Lugni et al. (2006). They observed three different impact modes: the impact of an incipient breaking wave, the impact of a broken wave with no phase mixing, and the impact of a broken wave with air/water mixing. Similar to the work of Lugni et al. (2006), in order to present the precise correlation of the particular flow (wave) configuration and the impact pressure for a wide range of frequency ratios, a detailed analysis of the flow structure and wave configuration is needed. This will be examined in future work.

Three-dimensional tank

In order to determine the dependence of sloshing in the 2-D tank on the natural frequency, a 3-D tank with the same filling ratio as the 2-D tank was considered in order to investigate the effect of natural frequency on sloshing. The time evolution of liquid motion, including the free surface deformation at regular intervals during one period (T) of the tank's surge motion for different natural frequency ratios, is shown in Fig. 9. It is comparable to that of the 2-D tank shown in Fig. 4. At fr_1, the roof impact and the sloshing of the liquid in the 3-D tank are more distinct than in the case of the 2-D tank, which can be clarified by comparing Figs. 4(a) and 9(a) for the 2-D tank and 3-D tank, respectively.

When the frequency ratio becomes fr_2, the deformation of the free surface in the 3-D tank over one period of tank surge motion reveals the same calm wave and very weak sloshing as in the 2-D tank. Therefore, these 3-D results, as shown in Fig. 9(b), confirm significant suppression of the sloshing at the second mode natural frequency of fr_2 observed in the 2-D results.

As fr increases from fr_2 to the higher modes of fr_3, fr_4, and fr_5, the free surface reveals irregular deformation with nonlinear waves at every instance, as shown in Figs. 9(c) to 9(e), respectively. However, the deformation of the free surface becomes weaker with higher natural frequency modes. Consequently, these 3-D results show an identical pattern of free surface deformation according to the natural frequency ratio compared to the 2-D results.

The values of the maximum free surface elevation (E_{Max}) of the 2-D and 3-D results are compared in Fig. 10, where the 3-D results contain only results of the natural frequency modes of fr_1, fr_2, fr_3, fr_4, and fr_5.

The maximum free surface elevation of the 3-D results presents almost the same variation according to the natural frequency mode as the results of the 2-D simulation. Namely, fr_1 has the maximum elevation with roof impact. Otherwise, the local minimum occurs at fr_2 among the frequency modes considered in this study. At other higher modes of fr_3, fr_4, and fr_5, the maximum free surface elevation has a local peak whose value decreases with increased natural frequency modes, as shown in Fig. 10.

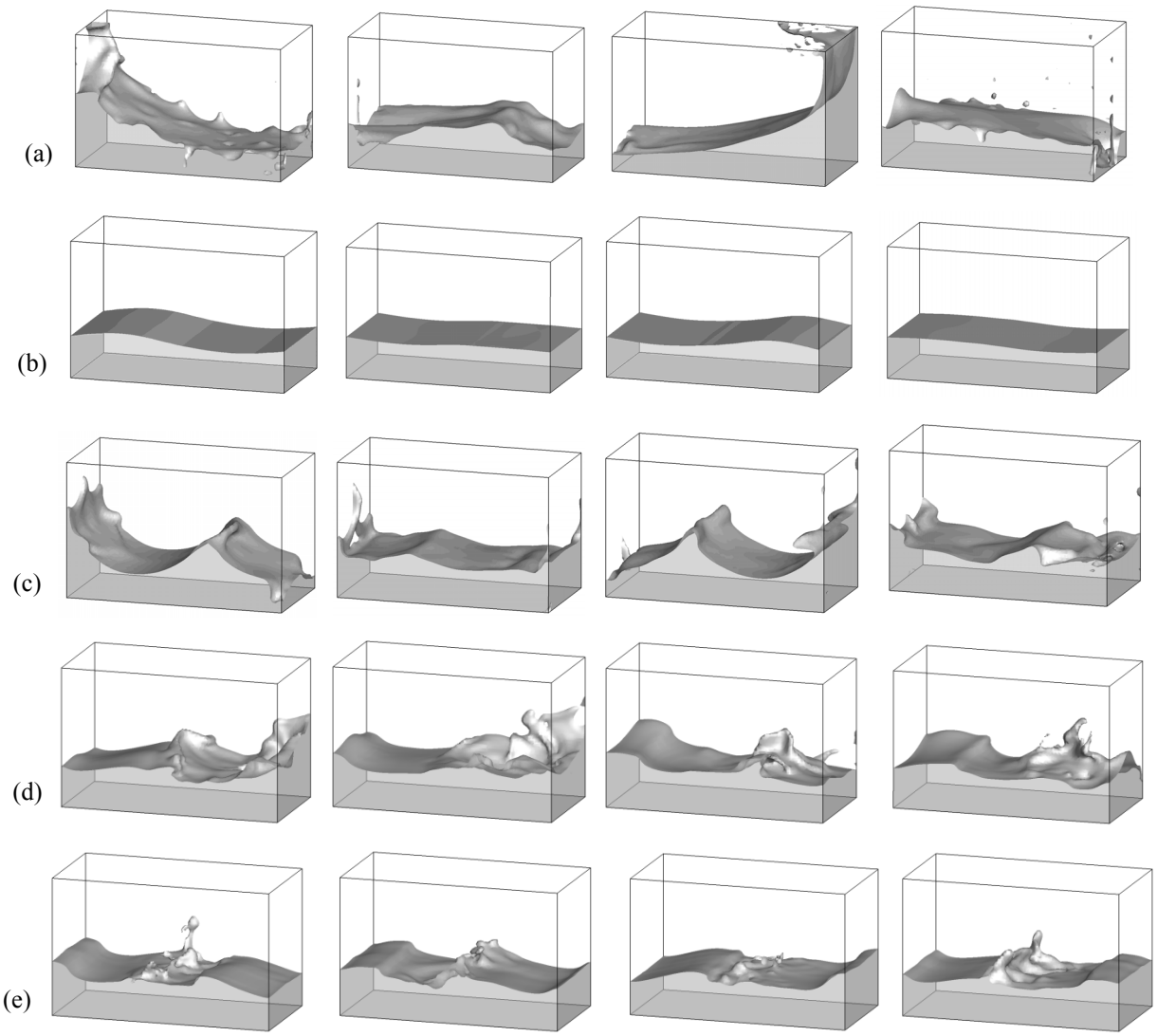

Fig. 9 Time sequences of free surface deformation at regular intervals during one period of tank surge motion for baffle heights of (a) fr_1, (b) fr_2, (c) fr_3, (d) fr_4, and (e) fr_5.

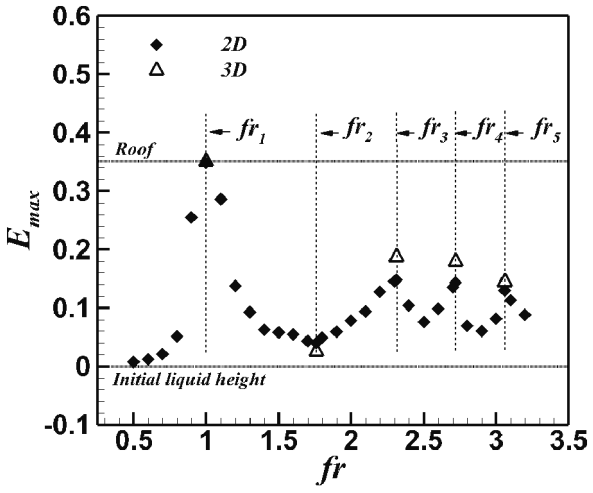

Fig. 10 Comparison of 2-D and 3-D results for the variation of averaged maximum free surface elevation according to frequency ratio.

However, the magnitude of E_{Max} of the 2-D and 3-D results is different. In general, the E_{Max} of the 2-D results is smaller than that of the 3-D results, as shown in Fig. 10(b). We suggest that this difference in E_{Max} between the 2-D and 3-D results originates from 3-D effects such as the swirl mode (Royon-lebeaud et al., 2007). The 3-D effect will be discussed in our comparison of the mean maximum 2-D and 3-D pressure later in detail.

The values of the mean maximum pressure ($P_{M,Max}$) of the 2-D and 3-D results are compared in Fig. 11. The $P_{M,Max}$ of the 2-D and 3-D results show almost the same dependence on the natural frequency mode. Also, this variation pattern of the maximum $P_{M,Max}$ according to the natural frequency mode is identical to that of E_{Max} shown in Fig. 10. At fr_1, $P_{M,Max}$ has the maximum value. The local minimum occurs at fr_2. At other higher modes of fr_3, fr_4, and fr_5, $P_{M,Max}$ has a local peak. However, $P_{M,Max}$ decreases with increased natural frequency modes.

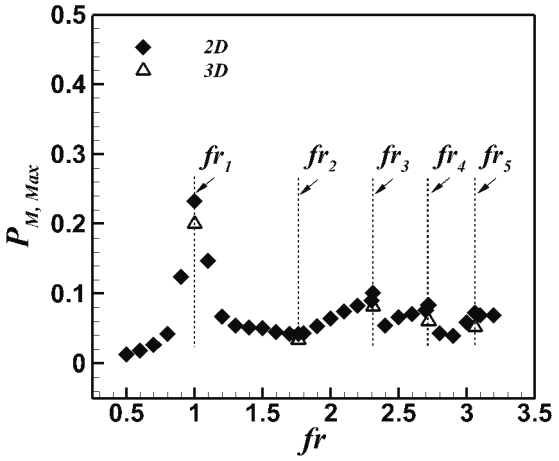

Fig. 11 Comparison of 2-D and 3-D results for the variation the mean maximum pressure ($P_{M,Max}$) according to frequency ratio.

The magnitude of $P_{M,Max}$ in the 2-D and 3-D results is different, especially at fr_1. In general, the $P_{M,Max}$ of the 2-D results is larger than that of the 3-D results, as shown in Fig. 10(b). We suggest that this difference in $P_{M,Max}$ between the 2-D and 3-D results originates from the 3-D effect. The evolution of the free surface in the 3-D simulations clearly reveals 3-D dependence, such as the wave deformation along the breadth and the broken wave. At fr_1, the swirl mode (Royon-lebeaud et al., 2007) as the 3-D effect is observed in Fig. 9(a) which can be identified by comparing the formation of the free surface of the 2-D results shown in Fig. 4(a).

This over-predicted pressure in the 2-D simulation can be compared with the gravity current and the drag force on a bluff body. The effect of rollup is much stronger in the two-dimensional simulations, since three-dimensionality helps to break up the spanwise or circumferential coherence. By considering the front of the heavy fluid to be a bluff body intruding into the light fluid, a crude analogy with the drag force on a cylindrical body subjected to crossflow can be drawn for which a 2-D model significantly overpredicts the drag force (Mittal and Balachandar, 1995).

Cantero et al. (2007) introduced these differences between 2-D and 3-D flow structures around a cylinder to explain the difference in the gravity current. The effect of three-dimensionality on the speed of the current can be significant. Thus, a weaker resistance to the flow can be expected in the case of a 3-D front than for the case of a coherent 2-D front, which could explain the faster spreading of 3-D currents (Cantero et al., 2007).

In the case of 3-D results, the concentration and the energy of the free surface becomes weaker and more dissipated, respectively, compared to the 2-D results. Therefore, the pressure that produces the impact force on the wall is smaller than that of the 2-D results.

CONCLUSION

We investigated the effect of natural frequency modes on liquid sloshing in 2-D and 3-D rectangular tanks by using a level set method based on the finite volume method. In order to examine the effect of a natural frequency mode on liquid sloshing,

we considered a wide range of frequency ratios ($0.5 \le fr \le 3.2$) that covers natural frequency modes ranging from 1 to 5. For all the cases considered in this study, the filling level is 30% of the tank height, and the tank motion is pure surge with the fixed excitation amplitude of 0.025 *L*.

As is well known, we can confirm that the first mode of the natural frequency of the fluid in a rectangular tank is distinctly the resonant frequency, based on our results for the free surface elevations for different frequency ratios.

Otherwise, at the second mode's natural frequency, a sudden increase in the amplitude of the free surface elevation does not occur. In particular, the local minimum peak of the free surface elevation appears at this frequency mode. This behavior of the free surface could be explained by the time sequence of the free surface deformation. Namely, at fr_2 and even though the second natural frequency mode, the deformation of the free surface revealed a calm wave and very weak sloshing. The liquid flows partially in the same direction as the tank motion, and partially in a direction that is opposite to the tank motion. Consequently, the waves undergo destructive interference. Some of the oscillation energy of the fluid is actually extracted by the opposing forces from the oscillation of the tank.

At the higher modes of fr_3 , fr_4 , and fr_5 , the free surface exhibits irregular deformation with nonlinear waves at every instance. However, the deformation of the free surface becomes weaker as the natural frequency mode increases.

The mean maximum wall pressure showed an identical pattern of free surface deformation according to the natural frequency ratio. The 3-D results confirmed the dependence of the free surface and the mean maximum wall pressure on the frequency ratio of the 2-D results.

However, the mean maximum wall pressure of the 2-D results is larger than that of the 3-D results, especially at the first mode of the natural frequency, which could be induced by the 3-D effect. For flow over a cylinder and the gravity current, the 2-D model significantly overpredicts the drag force, since three-dimensionality helps to break up the spanwise or circumferential coherence (Mittal and Balachandar, 1995; Cantero et al., 2007). Thus, in the 3-D results, the concentration and the energy of the free surface becomes weaker and more dissipated, respectively, compared to the 2-D results. As a result, the pressure as the impact force on the wall is smaller than that of the 2-D results.

In future work, a parametric study will be performed to investigate the effect of the frequency ratio on sloshing according to parameters such as the filling ratio and the excitation amplitude. Also, similar to the correlation of the particular flow (wave) configuration and the impact pressure presented by Lugni et al. (2006), detailed analyses of the flow structure and wave configuration are needed.

ACKNOWLEDGEMENT

This work was supported by a National Research Foundation of Korea (NRF) grant funded by the Korean government (MSIP) (no. 2011-0030662 and no. 2010-0025618).

REFERENCES

Akyildiz, H. and Unal, E., 2005. Experimental investigation of pressure distribution on a rectangular tank due to the liquid sloshing. *Ocean Engineering*, 32(11-12), pp.1503-1516.

Akyildiz, H. and Unal, N.E., 2006. Sloshing in a three-dimensional rectangular tank: numerical simulation and experimental validation. *Ocean Engineering*, 33(16), pp.2135-2149.

Armenio, V. and Rocca, M.L., 1996. On the analysis of sloshing of water in rectangular containers: numerical study and experimental validation. *Ocean Engineering*, 23(8), pp.705-739.

Bass, R.L., Bowles, E.B. and Cox, P.A., 1980. Liquid dynamic loads in LNG cargo tanks. *Society of Naval Architects and Marine Engineers*, 88, pp.103-126.

Bouscasse, B., Antuono, M., Colagrossi, A. and Lugni, C., 2013. Numerical and experimental investigation of nonlinear shallow water sloshing. *International Journal of Nonlinear Sciences and Numerical Simulation*, 14(2), pp.123-138.

Cantero, M.I., LEE, J.R., Balachandar, S. and Garcia, M.H., 2007. On the front velocity of gravity currents. *Journal of Fluid Mechanics*, 586, pp.1-39.

Chen, Y.G., Djidjeli, K. and Price, W.G., 2009. Numerical simulation of liquid sloshing phenomena in partially filled containers. *Computers & Fluids*, 38(4), pp.830-842.

Choi, H. and Moin, P., 1994. Effects of the computational time step on numerical solutions of turbulent flow. *Journal of Computational Physics*, 113(1), pp.1-4.

Delorme, L., Colagrossi, A., Souto-Iglesias, A., Zamora-Rodríguez, R., and Botía-Vera, E., 2009. A set of canonical problems in sloshing, Part I: Pressure field in forced roll-comparison between experimental results and SPH. *Ocean Engineering*, 36(2), pp.168-178.

Faltinsen, O.M., 1987. A numerical nonlinear method of sloshing in tanks with two dimensional flow. *Journal of Ship Research*, 22, pp.193-202.

Ibrahim, R.A., 2005. *Liquid sloshing dynamics: theory and applications*. New York: Cambridge University Press.

Jiang, G.S. and Peng, D., 2000. Weighted ENO schemes for Hamilton–Jacobi equations. *SIAM Journal on Scientific Computing*, 21, pp.2126-2143.

Jung, J.H., Yoon, H.S., Lee, C.Y. and Shin, S.C., 2012. Effect of the vertical baffle height on the liquid sloshing in a three-dimensional rectangular tank. *Ocean Engineering*, 44, pp.79-89.

Kang, D.H. and Lee, Y.B., 2005. *Summary report of sloshing model test for rectangular model, No. 001*. South Korea: Daewoo Shipbuilding & Marine Engineering Co., Ltd.

Kim, Y., 2013. Rapid response calculation of LNG cargo containment system under sloshing load using wavelet transformation. *Int. J. Nav. Archit. Ocean Eng*., 5(2), pp.227-245.

Kim, Y., Shin, Y. and Lee, K.H., 2005. Numerical study on sloshing-induced impact pressures on three-dimensional prismatic tanks. *Applied Ocean Research*, 26(5), pp.213-226.

Lee, C.S., Cho, J.R., Kim, W.S., Noh, B.J., Kim, M.H. and Lee, J.M., 2013. Evaluation of sloshing resistance performance for LNG carrier insulation system based on fluid-structure interaction analysis. *Int. J. Nav. Archit. Ocean Eng.*, 5(1), pp.1-20.

Lee, G.J., 2014. Moment of inertia of liquid in a tank. *Int. J. Nav. Archit. Ocean Eng.*, 6(1), pp.132-150.

Leonard, B.P., 1979. Stable and accurate convective modeling procedure based on quadratic upstream interpolation. *Computer Methods in Applied Mechanics and Engineering*, 19(1). pp.59-98.

Lugni, C., Brocchini, M. and Faltinsen, O.M., 2006. Wave impact loads: The role of the flip-through. *Physics of Fluids*, 18, pp.122101.

MacDonald, J. and Maguire, J., 2008. Lloyds Register's guidance on the operation of membrane LNG ships to avoid the risk of sloshing damage. *In: 23rd Gastech conference*, Bangkok, date(day month year), pp.

Mittal, R. and Balachandar, S., 1995. Effect of three-dimensionality on the lift and drag of nominally two-dimensional cylinders. *Phys. Fluids,* 7, pp.1841-1865.

Osher, S. and Sethian, J., 1988. Fronts propagating with curvature-dependent speed: algorithms based on Hamilton-Jacobi formulations. *Journal of Computational Physics*, 79, pp.12-49.

Peregrine, D.H., 2003. Water-wave impact on walls. *Annual review of fluid mechanics*, 35, pp.23-43.

Price, W.G. and Chen, Y.G., 2006. A simulation of free surface waves for incompressible twophase flows using a curvilinear level set formulation. *International Journal for Numerical Methods in Fluids*, 51(3), pp.305-330.

Rhee, S.H., 2005. Unstructured grid based Reynolds-averaged Navier–Stokes method for liquid tank sloshing. *Journal of Fluids Engineering Ameriacan Society of Mechanical Engineers*, 127(3), pp.572-582.

Royon-Lebeaud, A., Hopfinger, E.J. and Cartellier, A., 2007. Liquid sloshing and wave breaking in circular and square-base cylindrical containers. *J. Fluid Mech.*, 577, pp.467-494.

Sussman, M., Smereka, P. and Osher, S.A., 1994. Level set approach for computing solutions to incompressible two-phase flow. *Journal of Computational Physics*, 114, pp.46-159.

Wiesche, S., 2003. Computational slosh dynamics: theory and industrial application. *Computational Mechanics*, 30, pp. 374-387.

Wu, C.H. and Chen, B.F., 2009. Sloshing waves and resonance modes of fluid in a 3D tank by a time-independent finite difference method. *Ocean Engineering*, 36(6-7), pp.500-510.